2011 American Control Conference
on O'Farrell Street, San Francisco, CA, USA
June 29 - July 01, 2011

Pulse-Compression Probing for Nonlinear Systems with Additional Hard Nonlinearity at the Input

Matthew Ruschmann and N. Eva Wu

Abstract— **The effects of input hard nonlinearities on probing outputs are analyzed with respect to the pulse-compression probing method. The pulse-compression probing method identifies a local, linear model around an operating point of a nonlinear system by processing the system response to a probing input. The outputs of probing systems with one of six common input hard nonlinearities, including deadband, saturation, relay, backlash, and rate limit are derived. Pulse-compression probing is effective for the first five hard nonlinearities listed, where the probing outputs retain the same waveforms as if the probing inputs were scaled and offset. When probing an input with a rate limit, pulse-compression probing is effective when the bit duration of the probing input exceeds some threshold, which is based on the rate limit. As long as the probing input is properly designed with respect to the input nonlinearities present, the shape of the probing output is preserved. As a numerical example, pulse-compression probing method is applied to the NASA generic transport aircraft model with nonlinearities at the probing input.**

I. INTRODUCTION

The pulse-compression probing method identifies small-signal characteristics of a system at the probing output by processing the system's response to a probing input around an operating point. Thus, it provides a means for real-time health monitoring of nonlinear dynamic systems operating in the neighborhood of smooth nonlinearities. When input hard nonlinearities apply to the probing inputs, the identified small-signal characteristics change. The extent to which hard input nonlinearities affect probing outputs is discussed. Effects of six common nonlinearities are examined, and numerical examples of the method applied to an aircraft with input nonlinearities are discussed.

Previous applications of pulse-compression probing to linear time-invariant (LTI) systems include seismic exploration [1] and a linear hydraulic system [2]. Pulse-compression probing has also been applied to monitoring nonlinear dynamics of aerospace vehicles [3] by extracting from them small-signal characteristics at fixed operating points. Recently the pulse-compression probing method has been successfully applied to systems under dynamic operating conditions by monitoring the incremental output of the system [4], though the investigation in this paper does not consider this incremental implementation. Successful pulse compression probing relies on the design of a probing signal that effectively detects the change in a system without noticeable effects on the system operation. When a pseudo random binary sequence is used as the probing signal, the design amounts to selecting its magnitude, length (or order), and bit duration.

Much effort has been placed on the identification of nonlinear systems [5]. The majority of work concerning input hard nonlinearities provides methods for identifying the hard nonlinearity itself. The intention is often an adaptive mechanism that allows the controller to compensate for the nonlinearity [6]. Input nonlinearities pose a different challenge to the pulse-compression probing method which intends to encapsulate the system dynamics through the identified small-signal characteristics. Model-based fault diagnosis methods often compensate for known input nonlinearities by simulating them and processing their data using the altered input signal [7], and the concept extends readily to identifying linear systems with input nonlinearities.

Unlike these traditional methods, the pulse-compression probing method requires a specific probing input to be injected into the system. The presence of an input nonlinearity alters the system response to the small-signal probing input in ways determined by the particular nonlinearity involved. The six specific hard nonlinearities that are considered in this paper belong to ranges of neutral signal input/output relationship, input rate limit saturations, and hysteresis [8]. The effects of each hard nonlinearity on pulse-compression probing is derived, and proper design of the probing sequence is discussed for each scenario.

Numerical results of pulse-compression probing for monitoring the longitudinal dynamics of the NASA generic transport aircraft model (GTM) are reported. Examples of each nonlinearity are presented individually at the probing input, and the effects on the probing outputs are discussed. The GTM is a high fidelity, nonlinear Simulink model of a dynamically scaled small unmanned aerial vehicle developed by NASA to investigate modeling and control of large transport vehicles in upset conditions [9]. Pulse-compression probing is used to monitor the GTM by detecting changes of the probing output in real-time. Reliable change detection of vehicle dynamics in real-time is crucial to the safety of flight.

The remaining sections are organized in the following manner. Section II reviews the pulse-compression probing method applied to identification of small-signal characteristics of a nonlinear system around an operating point. Examples of input hard nonlinearities are introduced in Section III, and their effects on the probing outputs are

This work was supported in part by NASA Under Grant NNX08AC65A.

Matthew Ruschmann is a post-doctoral research scientist with the Department of Electrical and Computer Engineering, Binghamton University, Binghamton, NY 13902, mruschm2@binghamton.edu

N. Eva Wu is with the Department of Electrical and Computer Engineering, Binghamton University, Binghamton, NY 13902, evawu@binghamton.edu

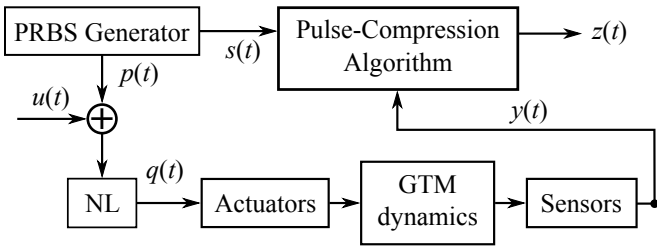

Fig. 1. Signal flow diagram with injection and pickup points of probing input p and output z with probing reference s for monitoring the NASA GTM, where r is the command input and y is the measured output. NL is a block containing one of the hard nonlinearities to be discussed in Section III.

analyzed. Requirements on the probing input for effective system monitoring are discussed. In Section IV, numerical examples of the pulse-compression probing method with a probing input subject to hard nonlinearities are discussed using the NASA GTM as a test bed. Section V concludes the paper.

II. Review of Pulse-Compression Probing Method

The pulse-compression probing method can be and has been applied to identify pulse responses, or Markov parameters, of linear time-invariant systems online without the need for a parametric model [2]. The method applies equally well to extract small-signal pulse responses of nonlinear systems at fixed operating conditions [10], [11]. In this section, the probing output for small-signal pulse response using pulse-compression probing is reviewed in the discrete-time domain. The material in this section draws significantly from the derivation for linear time-varying systems in [4].

A. Overview of the pulse-compression principle

The pulse-compression probing method is intended to recover a system's pulse response at the probing output $z(t)$ in response to an injected probing input $p(t)$ around a set point, as shown in Fig. 1. Consider a causal time-invariant system with a small-signal pulse response $h(i)$ around an operating point, where i is the ith tap of the response sequence. Assume that the memory length of the pulse response is bounded by M, i.e., $h(i) = 0$, $i \geq M-1$. This imposes a stability requirement on the system, which is discussed in [4].

Define the probing output in discrete time as

$$z(k) = h(k) * p(k) \otimes s(k) = y(k) \otimes s(k) \tag{1}$$

where $*$ represents convolution, $\otimes$ represents correlation, $s(k)$ is a reference signal, and $y(k)$ is the system output of the LTI system. The pulse response is shift-invariant, thus

$$\begin{aligned} z(k) &= [h(k) * p(k)] \otimes s(k) \\ &= h(k) * [p(k) \otimes s(k)] \\ &= h(k-M) \end{aligned} \tag{2}$$

provided that $s(k)$ and $p(k)$ are specially designed so that

$$p(k) \otimes s(k) = \delta(k-M) \tag{3}$$

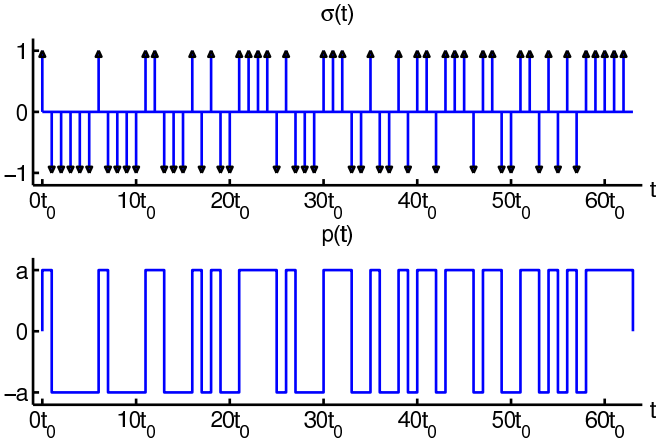

Fig. 2. An impulsive PRBS $\sigma(t)$ of order $n = 6$, and a continuous-time probing signal $p(t)$ generated by convolving it with a narrow rectangular wavelet of with t_0 equal to the bit duration.

where $\delta(i)$ is the Kronecker delta function.

The goal of probing signal design is to minimize both the noise at system output $y(k)$, caused by probing input $p(k)$, and the noise at probing output $z(k)$, caused by control signal $u(k)$. It can be achieved by ensuring $p(k) \otimes s(k) \approx \delta(k-M)$ as close as possible. $p(k)$ and $s(k)$ are designed from $\sigma(k)$. $\sigma(k)$ can be selected as a single period of a pseudo-random binary sequence (PRBS) of order n satisfying $M = 2^n - 1$, bit duration t_0, and unit amplitude.

The injected probing signal, $p(k)$, can be selected to be a digital, cyclically repeating copy of $\sigma(k)$ with magnitude a. The reference signal, $s(k)$, can be selected to be a cyclic repetition of $\sigma(k)$ with unit magnitude. Fig. 2 shows an example of continuous-time versions of $\sigma(k)$ and $p(k)$ for $n = 6$. The PRBS period $T = Mt_0 = (2^n - 1)t_0$ corresponds to the memory length of impulse response $h(t)$ which vanishes when $t \geq T$. The specifics on the design of $\sigma(k)$ including equations to calculate n, t_0, and a for an LTI system can be found, for example, in [2].

B. Probing output in discrete time

The pulse-compression probing algorithm is carried out in discrete time. With $M = 2^n - 1$, the number of non-zero taps in an nth order PRBS [12], [13], the system output $y(k) = h(k) * p(k)$ is the convolution of the probing signal, $p(k)$, with the small-signal pulse response $h(k)$. This can be computed by summing the system's response to each individual pulse of p at the time instance k,

$$y(k) = \sum_{j=0}^{M-1} h(j)p(k-j) \tag{4}$$

where $p(k) = p(k+M)$ is assumed as it cyclically repeats.

A single period of $y(k)$ is correlated with the reference $s(k)$ to observe a complete M-tap probing output, which is given by

$$z(k) = y(k) \otimes s(k) = \sum_{i=0}^{M-1} y(k-i)s(M-1-i). \tag{5}$$

Substituting (4) into (5) yields

$$z(k) = \sum_{i=0}^{M-1} \left\{ \sum_{j=0}^{M-1} \left[p(k-i-j)h(j) \right] s(M-1-i) \right\}. \quad (6)$$

The term $p(k-i-j)s(M-1-i) = a$ when $(k-j \mod M) = M-1$ based on the probing signal and reference signal design. Therefore, $aMh(k \mod M)$ can be extracted from the two summations of (6). The remaining terms sum to $-a$ as the coefficient for all remaining taps of the pulse response, and

$$z(k) = a \left[(M)h(k \bmod M) - \sum_{j=0, j \neq k \bmod M}^{M-1} h(j) \right]. \quad (7)$$

The negative terms of (7) result in a small error when identifying the $(k \bmod M)$th tap. (7) can be rewritten to remove the exclusion from the summation,

$$z(k) = a \left[(M+1)h(k \bmod M) - \sum_{j=0}^{M-1} h(j) \right]. \quad (8)$$

In (8), it is apparent that for a system with zero DC component, $\sum_i h(i) = 0$, the errors cancel themselves. Alternatively, the errors can be corrected by modifying the probing output,

$$\zeta(k) = z(k) + \sum_{j=0}^{M-1} z(k-j) = a(M+1)h(k \bmod M). \quad (9)$$

III. Pulse-Compression Probing with Hard Nonlinearities at the Input

The usefulness of the probing output to change detection is investigated when the probing input signal, $p(t)$, is subject to various hard nonlinearities. This is accomplished through comparison, using the same probing input, of the probing output without hard nonlinearities present to probing output with an input nonlinearity present. Previous work on pulse-compression probing has always assumed a non-empty open set around the operating point, over which the nonlinearity has a smooth first derivative. Six hard nonlinearities are reviewed, and the individual effects of each nonlinearity on the probing output are analyzed. Five of six nonlinearities only affect the scaling and offset of the probing signal. Analysis of the last nonlinearity is limited by the assumption of discrete, sampled calculations.

A. Scaling and Offset of the Probing Signal

The scaling and shifting effects of nonlinearities on the probing signal are investigated along with the corresponding effects on probing output. In Fig. 1, the probing signal, $p(t)$, is modified by the nonlinearity block, NL. For simplicity and clarity of presentation, it is assumed that the system is trimmed to an equilibrium position such that small signal analysis is conducted around a steady-state value of control $u(t)$ resulting in a steady-state measured output. In [3], the small-signal characteristics are extracted by subtracting the trim condition from the measured outputs using a reference model. Then it can be assumed that $u(t) = 0$ for small-signal analysis, and $q(t)$ is the direct result of the nonlinearity in block NL applied to $p(t)$.

For five of the considered nonlinearities, the probing input appears to be scaled and shifted to a new apparent amplitude, $\tilde{a}$, and an apparent offset, $\tilde{b}$. Analytically,

$$q(t) = \frac{\tilde{a}}{a} p(t) + \tilde{b}. \quad (10)$$

To quantify the effects of nonlinearity on the probing output, (10) replaces $p(k)$ in (4). The resulting probing output is

$$\bar{z}(k) = \tilde{a} \left[(M+1)h(k \bmod M) - \sum_{j=0}^{M-1} h(j) \right] + \tilde{b} \sum_{j=0}^{M-1} h(j). \quad (11)$$

After compensating for the errors introduced by a possible non-zero DC component,

$$\bar{\zeta}(k) = \bar{z}(k) + \sum_{j=0}^{M-1} \bar{z}(k-j) = \tilde{a}(M+1)h(k \bmod M) + \tilde{b} \sum_{j=0}^{M-1} h(j). \quad (12)$$

In both cases, the primary source of error is the last term related to offset $\tilde{b}$ for systems with a DC component.

B. Hard Nonlinearities and the Effects on Probing Output

This section reviews six hard nonlinearities to each of which the probing input (10) is applied as demonstrated in Fig. 1. The first five nonlinearities can be interpreted in terms of the apparent probing signal in Section III-A. The remaining nonlinearity has more complicated effects, which are simulated and discussed.

1) Deadband: A deadband is a range of input signal where no output signal occurs. Deadbands can result from both electrical and mechanical effects, i.e. friction [14]. They are sometimes introduced purposefully to reduce oscillation of feedback control [15]. A deadband is defined by $d_- \leq 0$ to $d_+ \geq 0$ such that input p to the nonlinearity results in the following output q:

$$q = \begin{cases} p + d_- & \text{when } p < d_-, \\ 0 & \text{when } d_- \leq p \leq d_+, \\ p - d_+ & \text{when } p > d_+. \end{cases} \quad (13)$$

A visualization of this relationship is presented in Fig. 3a.

Given a deadband from d_- to d_+ in block NL of Fig. 1, the effects can vary depending on the limits of the deadband. Consider that the probing input is centered around zero, then the six following scenarios are possible:

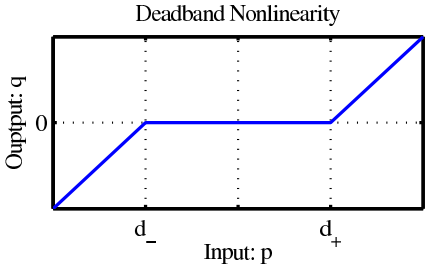

(a) A visualization of the input-output relationship for a deadband nonlinearity.

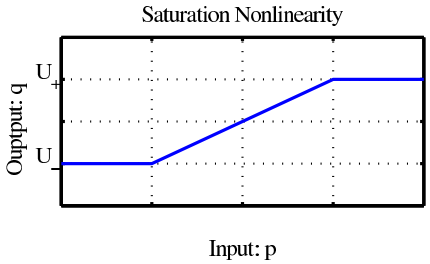

(b) A visualization of the input-output relationship for saturation nonlinearities.

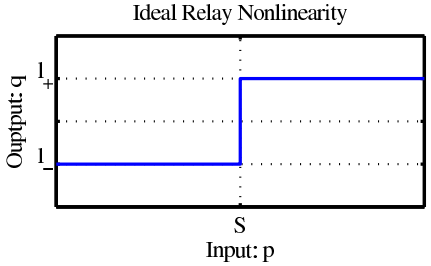

(c) A visualization of the input-output relationship for a relay nonlinearity.

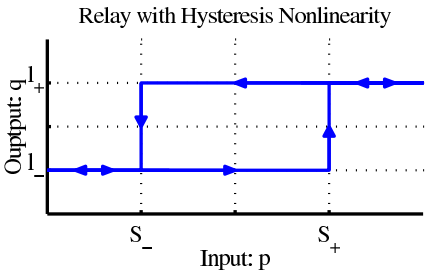

(d) The input-output relationship for a relay with hysteresis. Arrows indicate separate paths based on the direction of the input signal.

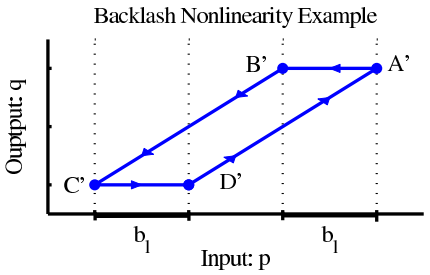

(e) An example of the input-output relationship for hysteresis defined by b_l. The arrows indicate the output path as the input changes from A' to B' to C' to D' back to A'.

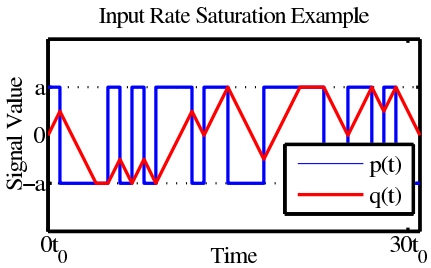

(f) Plot of an example input signal, $p(t)$, and the effects of a slow rate limit, $r_l = 0.5\frac{a}{t_0}$.

Fig. 3. Input-output relationships or input-output examples for each of the six hard nonlinearities considered.

a. If $d_+ < -a$ or $d_- > a$, then the deadband has no effect on the probing output.
b. If $d_+ = -d_- < a$, then the apparent probing output in (10) is defined by $\tilde{a} = a - d_+$ and $\tilde{b} = 0$.
c. If $d_+ \neq d_-$, $d_+ < a$ and $d_- > -a$, then the apparent probing output in (10) is defined by

$$\tilde{a} = \frac{a - d_+ + d_- + a}{2} = a - \frac{d_+}{2} + \frac{d_-}{2}, \qquad (14)$$

$$\tilde{b} = a - d_+ - \tilde{a} = -\frac{d_+}{2} - \frac{d_-}{2}. \qquad (15)$$

d. If $d_+ \neq d_-$, $d_+ > a$ and $d_- > -a$, then the effective probing output in (10) is defined by $\tilde{a} = \frac{d_- + a}{2} = \frac{a}{2} + \frac{d_-}{2}$ and $\tilde{b} = 0 - \tilde{a} = -\frac{d_-}{2} - \frac{a}{2}$.
e. If $d_+ \neq d_-$, $d_+ < a$ and $d_- < -a$, then the effective probing output in (10) is defined by $\tilde{a} = \frac{a - d_+}{2} = \frac{a}{2} - \frac{d_+}{2}$ and $\tilde{b} = a - d_+ - \tilde{a} = \frac{a}{2} - \frac{d_+}{2}$.
f. If $d_+ > a$ and $d_- < -a$, then the apparent probing input in (10) has $\tilde{a} = 0$ and $\tilde{b} = 0$. The probing output will be zero. The amplitude of the probing input must be increased for any identification to occur.

If the limits of the deadband are known, then the effects could be compensated for as long as $d_- > -a$ or $d_+ < a$.

2) Input saturation: An input saturation point is a bound on either the upper or lower value of an input. Saturation points often represent limits on the output of electrical systems, i.e. amplifiers, or mechanical systems, i.e. fluid powered cylinders, [8]. An input saturation defined by two points, U_- and U_+ where $U_- < U_+$, has the following output q for input p:

$$q = \begin{cases} U_- & \text{when } p \leq U_-, \\ p & \text{when } U_- < p < U_+, \\ U_+ & \text{when } p \geq U_+. \end{cases} \qquad (16)$$

A visualization of this relationship is presented in Fig. 3b

Given input saturation points U_- and U_+ where $U_- < U_+$ in block NL of Fig. 1, the effects can be summarized by the following five situations using the apparent probing input in (10):

a. If $U_- < -a$ and $a < U_+$, then $\tilde{a} = a$ and $\tilde{b} = 0$. The saturation points have no effect on probing output.
b. If $U_- > -a$ and $U_+ < a$, then $\tilde{a} = \frac{U_+ - U_-}{2}$ and $\tilde{b} = U_+ - \tilde{a} = \frac{U_+ + U_-}{2}$.
c. If $U_- > -a$ and $U_+ > a$, then $\tilde{a} = \frac{a - U_-}{2}$ and $\tilde{b} = a - \tilde{a} = \frac{a + U_-}{2}$.
d. If $U_- < -a$ and $U_+ < a$, then $\tilde{a} = \frac{U_+ + a}{2}$ and $\tilde{b} = U_+ - \tilde{a} = \frac{U_+ - a}{2}$.
e. If $U_- > a$ or $U_+ < -a$, then $\tilde{a} = a$ and $\tilde{b} = 0$. Probing output is zero.

The most obvious solution is to avoid any known saturation points, $U_- < -a$ and $a < U_+$. If saturation points are known, the probing output can be adjust accordingly as long as $U_- < a$ and $U_+ > -a$.

3) Ideal relay: An ideal relay is described by the following switching function that is also presented in Fig. 3c:

$$\mathrm{f}(u) = \begin{cases} l_+, & \text{if } u > S \\ \frac{l_+ - l_-}{2}, & \text{if } u = S \\ l_-, & \text{if } u < S. \end{cases} \qquad (17)$$

The relay characteristic models switching devices, i.e electromechanical relays and thyristor circuits [16]. l_- and l_+ can also represent two levels of quantization to provide some understanding of the effects of quantization on a relatively small probing input.

Given that the NL block of Fig. 1 is an ideal relay described by (17), the apparent probing input of (10) is described by $\tilde{a} = \frac{l_+ - l_-}{2}$ and $\tilde{b} = \frac{l_+ + l_-}{2}$ if $-a < S < a$. If $S < -a$ or $S > a$, then there is no probing output, $\tilde{a} = 0$, $\tilde{b} = l_-$ or $\tilde{a} = 0$, $\tilde{b} = l_+$, respectively.

4) Relay with hysteresis: Some non-ideal relays do not switch at the same point in both directions. These relays must overcome some hysteresis, or delay dependent on memory within the system, $S_+ > S$ before switching to l_+ and $S_- < S$ before switching to l_-. A visual description of the delay is presented in Fig. 3d using arrows to indicate the path of the output as the input changes in either direction.

With this nonlinearity, the apparent probing input is the same as the ideal relay if $S_- > -a$ and $S_+ < a$. If these conditions are not meant, then there is not probing output, $\tilde{a} = 0$ and the value of $\tilde{b}$ depends on the value of the system's memory.

5) Backlash: The backlash characteristic models clearance between mating components. For example, gears must overcome a small clearance between teeth [17]. Eliminating this slack runs the risk of jamming gears. Backlash is a specific example of hysteresis [8]. For example, backlash in a gear can be described by the gap between meshing teeth, b_l. If input p reverses direction, then the touching teeth separate, and a deadband of width $d_+ - d_- = b_l$ must be overcome before the teeth are touch again.

For example, examine the input-output path in Fig. 3e. As the input changes from A' to B', it must overcome backlash b_l representing the gap between meshing teeth. When B' is reached, the gear teeth touch until the gear direction is reversed at C'. The gap is overcome from C' to D', and the process repeats when it reverses directions again at A'.

Backlash with magnitude b_l is introduced into NL of Fig. 1. This results in the apparent probing input of (10) described by $\tilde{a} = \max(0, a - \frac{b_l}{2})$ and $\tilde{b} = 0$. If the magnitude of the backlash in known and $2a > b_l$, then the effects are easily compensated for.

6) Input rate saturation: To simplify analysis, it is often assumed that values can change instantaneously. The reality is that these changes are all subject to some rate limit. Input rate saturation is defined by a value r_l. The nonlinearity results in an output signal q that follows input p where $\frac{dq}{dt} \leq r_l$ is enforced. Often this limit is so high that it can be ignored without consequence. However, the pulse-compression probing method relies on fast sampling and a quickly changing probing input, which may test the bound on input rate saturation.

The effects of input rate saturation cannot be equated to (10). Instead, an intuitive analysis is presented. Observations indicate that probing output becomes corrupted when the rate limit is low enough that peeks of single bit duration changes in the probing signal are truncated corrupting the probing input and resulting in transients. This is exemplified in Fig. 3f. A limit on the input rate saturation can be derived from $0 < \frac{dq}{dt} \leq r_l$ by integrating over a single bit duration:

$$\int dq \leq \int_0^{t_0} r_l dt, \tag{18}$$

$$q(t_0) - q(0) \leq r_l(t_0 - 0). \tag{19}$$

For a positive transition from $q(0) = -a$ to $q(t_0) = a$ over a single bit duration, the bound on rate limit is derived as

$$2a \leq r_l t_0 \tag{20}$$

$$r_l \geq 2\frac{a}{t_0}. \tag{21}$$

Observations indicate that as $r_l << 2\frac{a}{t_0}$, the probing output becomes noisier.

IV. Results of On-line Probing with Hard Nonlinearities Applied to the Probing Input

The results of probing the elevators of the NASA GTM [18] are plotted with various individual hard nonlinearities applied to the probing input. The NASA GTM is a high-fidelity nonlinear model, but the nonlinearities are primarily smooth with the exception of an extremely high rate limit in the actuators. This rate limit has been insignificant in previous investigations. Probing of the GTM has been investigated at both fixed [3] and dynamic [4] operating conditions. This section expands on previous works by investigating hard nonlinearities within an open-loop GTM simulation.

A block diagram of the open-loop GTM simulation with pulse-compression probing implemented is provided in Fig. 1. The GTM is simulated on a trimmed, straight and level flightpath. The probing signal is injected into the elevator control. For clarity of presentation, the probing output is monitored at only one output channel, the aircraft pitch θ, because the effects of elevator control on this channel are significant. Although, the probing output could be monitored at any system output. The probing input is designed with bit duration $n = 9$, memory length $T = 5.110$sec, bit duration $t_0 = 0.010$sec, and probing signal amplitude $a = 0.005$deg, which is not modified to compensate for hard nonlinearities.

The results of probing various nonlinearities are summarized in Fig. 4, which compares the probing outputs when hard input nonlinearities are present to previous results without hard nonlinearities. The deadband applied to the example in Fig. 4a causes the probing input to appear as $\tilde{a} = \frac{2}{3}a$ and $\tilde{b} = 0$. A corresponding drop in the magnitude of the probing output by $\frac{1}{3}$ is correctly observed. The input saturation applied in Fig. 4b causes the probing input to appear as $\tilde{a} = \frac{a}{2}$ and $\tilde{b} = -\frac{a}{2}$. A drop in magnitude of the probing output is observed, but the offset is not observed because the elevator to pitch channel of the GTM has small DC component. Likewise, the relay and backlash demonstrate similar results in Fig. 4c and Fig. 4d, respectively.

The effects of input rate saturation are investigated in Fig. 4e and Fig. 4f. In Fig. 4e the rate limit only slightly violates

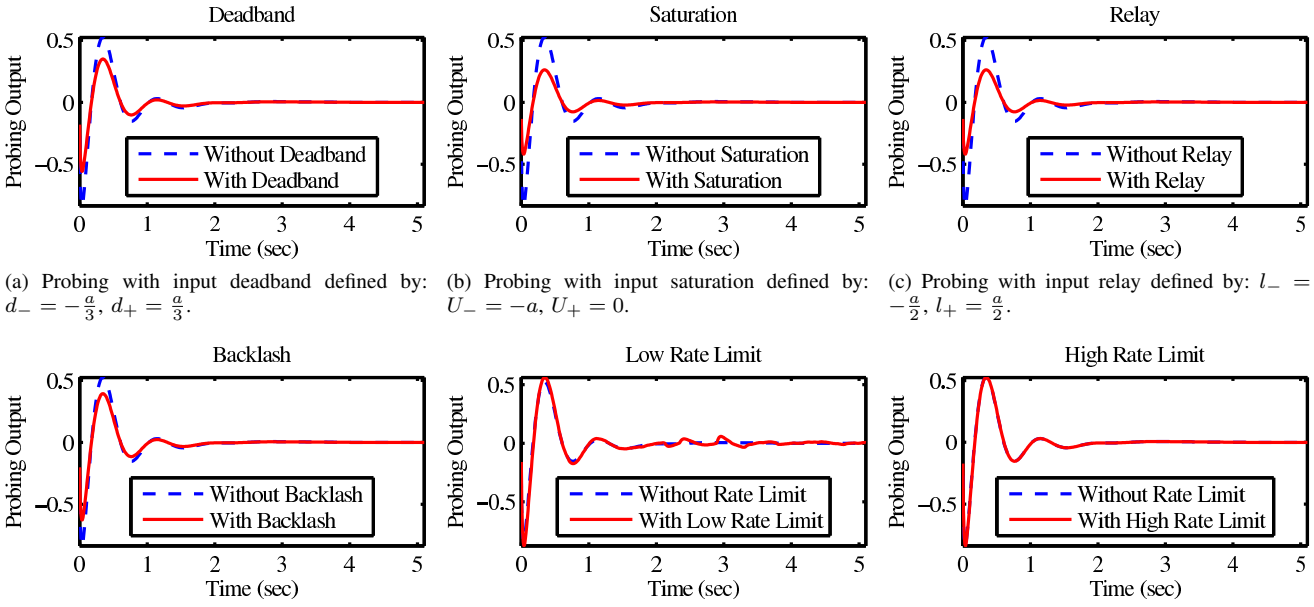

(a) Probing with input deadband defined by: $d_- = -\frac{a}{3}$, $d_+ = \frac{a}{3}$.

(b) Probing with input saturation defined by: $U_- = -a$, $U_+ = 0$.

(c) Probing with input relay defined by: $l_- = -\frac{a}{2}$, $l_+ = \frac{a}{2}$.

(d) Probing with backlash defined by: $b_l = \frac{a}{2}$.

(e) Probing with low input rate limit $r_l = \frac{1.8a}{t_0}$.

(f) Probing with high input rate limit $r_l = \frac{2a}{t_0}$.

Fig. 4. Results of probing elevators of the GTM with various nonlinearities present at the input. Probing output is processed at the measured pitch angle, θ, in radians. Details about the nonlinearity implemented in each example are given in the subplot titles.

$r_l \geq 2\frac{a}{t_0}$, and the observed probing output is slightly noisy in the tail. The noise can be resolved by probing with a slower PRBS bit duration, if acceptable. In Fig. 4f $r_l = 2\frac{a}{t_0}$, and the probing output is very accurate.

V. CONCLUSIONS

The pulse-compression probing method is shown to be resilient to six hard input nonlinearities. A simple analysis of five nonlinearities shows that the nonlinearities scale and offset the probing output, but they do not alter the basic shape of the probing output. Furthermore, the effects of these five input nonlinearities can be compensated for at the probing output if the parameters of the nonlinearities are known. The sixth nonlinearity, input rate saturation, causes noisy probing outputs in simulations if the rate limit is slower than some bound, which is defined in by the rate limit.

VI. ACKNOWLEDGMENTS

The authors thank the reviewer of [3] who recommended an investigation into hard nonlinearities for the pulse-compression method.

REFERENCES

[1] H. Chen and N.E. Wu, "Method of High Resolution and High SNR Data Acquisition for Probing Using Pulse-Compression," US Patent 5,426,618, June, 1995.

[2] N.E. Wu and X. Wang, "A Pulse-Compression Method for Process Monitoring," *Proceedings of the American Control Conference*, pp. 2127–2130, Arlington, VA, 2001.

[3] N.E. Wu, M.C. Ruschmann, J. Huang, and K. Huang, "Probing the NASA Generic Transport Aircraft in Real-Time for Health Monitoring," *IEEE Transactions on Control System Technology*, August, 2010, accepted and awaiting publication.

[4] M.C. Ruschmann, J. Huang, and N.E. Wu, "Pulse-Compression Probing of Small Signal Characteristics for Nonlinear Systems in Dynamic Operating Conditions," *Proceedings of the 49th IEEE Conference on Decision and Control*, pp. 1593–1599, Atlanta, GA, 2010.

[5] J. Sjöberg, Q. Zhang, L. Ljung, A. Benveniste, B. Delyon, P. Glorennec, H. Hjalmarsson, and A. Juditsky, "Nonlinear Black-Box Modeling in System Identification: A Unified Overview," *Automatica*, vol. 31, no. 12, pp. 1691–1724, 1995.

[6] G. Tao and P. Kokotovic, *Adaptive Control of Systems with Actuator and Sensor Nonlinearities*. John Wiley & Sons, Inc. New York, NY, 1996.

[7] P. Frank, "Fault Diagnosis in Dynamic Systems Using Analytical and Knowledge-Based Redundancy: A Survey and Some New Results," *Automatica*, vol. 26, no. 3, pp. 459–474, 1990.

[8] H. Khalil, *Nonlinear Systems*. Prentice Hall, Upper Saddle River, NJ, 2002.

[9] T. Jordan, J. Foster, R. Bailey, and C. Belcastro, "AirSTAR: A UAV Platform for Flight Dynamics and Control System Testing," *25th AIAA Aerodynamic Measurement Technology and Ground Testing Conference*, San Fransisco, CA, 2006.

[10] K. Huang, J. Huang, and N.E. Wu, "Verification of a Small Signal Probing Concept for Prognosis on a Nonlinear Model for Longitudinal Motion of a Boeing-747," *Proceedings of the American Control Conference*, pp. 4165–4170, St. Louis, MO, 2009.

[11] M.C. Ruschmann, J. Huang, and N.E. Wu, "Probing the NASA Generic Transport Aircraft in Real-Time for Health Monitoring," *Proceedings of the Combined 48th IEEE Conference on Decision and Control and 28th Chinese Control Conference*, pp. 4920–4926, Shanghai, China, 2009.

[12] J.G. Proakis, *Digital Communication*. McGraw-Hill, 2001.

[13] R. Ziemer and R. Peterson, *Introduction to Digital Communication*. Prentice Hall, Upper Saddle River, NJ, 2001.

[14] B. Armstrong-Hélouvry, P. Dupont, and C. De Wit, "A Survey of Models, Analysis Tools and Compensation Methods for the Control of Machines with Friction," *Automatica*, vol. 30, no. 7, pp. 1083–1138, 1994.

[15] C.W. Taylor, K.Y. Lee, and D.P. Dave, "Automatic Generation Control Analysis with Governor Deadband Effects," *IEEE Transactions on Power Apparatus and Systems*, pp. 2030–2036, 1979.

[16] Q. Wang, T. Lee, and C. Lin, *Relay Feedback: Analysis, Identification, and Control*. Springer Verlag, 2003.

[17] D. W. Dudley, *Handbook of Practical Gear Design*. CRC Press LLC, Boca Raton, FL, 1994.

[18] D. Cox, "The GTM DesignSim r415", 2008.